Journal of Power Sources 264 (2014) 254–261

Contents lists available at ScienceDirect

Journal of Power Sources

journal homepage: www.elsevier.com/locate/jpowsour

A simple modification of near-infrared photon-to-electron response with fluorescence resonance energy transfer for dye-sensitized solar cells

Liang Li [a], Yulin Yang [a,*], Ruiqing Fan [a,*], Yanxia Jiang [a], Liguo Wei [a], Yan Shi [a], Jia Yu [a], Shuo Chen [a], Ping Wang [a], Bin Yang [b], Wenwu Cao [b,c]

[a] Department of Chemistry, Harbin Institute of Technology, Harbin 150001, China
[b] Condensed Matter Science and Technology Institute, Harbin Institute of Technology, Harbin 150080, China
[c] Materials Research Institute, The Pennsylvania State University, University Park, PA 16802, USA

HIGHLIGHTS

- UC-YF_3 is utilized as an attachment layer in DSSC.
- UC-YF_3 as light scattering layer achieve a higher power-conversion efficiency.
- FRET and FRET-like process are found in the modified DSSC.
- The NIR-photon to electron process is confirmed by SPS and IPCE.

GRAPHICAL ABSTRACT

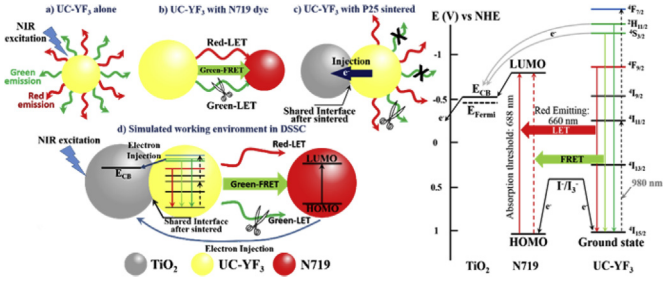

ARTICLE INFO

Article history:
Received 11 February 2014
Received in revised form
1 April 2014
Accepted 17 April 2014
Available online 30 April 2014

Keywords:
Upconversion
Fluorescence resonance energy transfer
Electron injection
Dye-sensitized solar cells

ABSTRACT

Upconversion (UC) Er, Yb-YF_3 is introduced into dye-sensitized solar cells (DSSC) through a simple method to investigate the effect of UC particles in photoanode. The utilization of UC phosphor can significantly improve the photocurrent of the cells under both infrared irradiation and sunlight. Fluorescence resonance energy transfer (FRET) and luminescence-mediated energy transfer between UC-YF_3 and N719 dye are explored as the main contribution that UC-YF_3 made to DSSC. With the multi-efforts of UC-YF_3, power conversion efficiency (PCE) of DSSC is improved from 5.18% to 6.22%. Besides, Electron transfer between UC-YF_3 and TiO_2 is found after sintered at 450 °C, and the PCE value of DSSC is improved further (5.34% → 6.76%). In addition, we explore that UC-YF_3 can serve as a scattering material to increase the light absorption capability of the cells and increase the photocurrent of the cells under simulated sunlight irradiation.

1. Introduction

As a clean and sustainable energy, solar energy has been the most active research area in the energy field in recent years. Owning to their low cost, environmental friendliness, simple production processes, and high efficiency, dye sensitized solar cells (DSSCs) have brought a revolutionary innovation for photoelectrochemical solar cell, and blazed a direction for new-generation solar cells since it was first reported in 1991 by Gratzel's group [1–3]. However, absorption spectra of dyes N3 and N719 which is usually used as standard photosensitized agents do not perfectly match the solar spectrum [4–6]. Photons with lower

* Corresponding authors. Tel.: +86 451 86413710; fax: +86 451 86418270.
E-mail addresses: ylyang@hit.edu.cn (Y. Yang), fanruiqing@hit.edu.cn (R. Fan).

http://dx.doi.org/10.1016/j.jpowsour.2014.04.100
0378-7753/

energy (such as NIR light) transmit through the DSSC without any contribution to the electrical output, because these photons are transparent to the dye. Most of the NIR radiations are in the shorter NIR wavelength regions. Of the 52% total solar energy delivered in the NIR region (700–2500 nm), 50% is within the wavelength of 700–1000 nm; 30% lies within the wavelength of 1000–1500 nm; and 20% lies within the wavelength of 1500–2500 nm [7,8]. Although many novel dyes with wide absorption spectra have been reported in the literature [9,10], high cost, complicated production process, as well as low yield limited further improvement of the power conversion efficiency (PCE) of DSSC. A useful method for reducing the transmission loss of photons with lower energy (especially NIR light) is upconverting the low-energy photons into higher-energy-photons, which can be help increase the efficiency of DSSCs [11].

Upconversion materials can generate one high-energy-photon by absorbing two or more low-energy-photons, which is called anti-stokes emission [12,13]. Efficient upconversion photoluminescence from nanoparticles has tremendous potential in application as sunlight-modifier for enhancing efficiency of DSSCs [14]. Typical DSSC systems with upconversion materials are illustrated in Fig. 1, in which rare earth-doped upconversion materials are used for photovoltaic applications. As structured in Fig. 1a, the UC-layer could modify the incident solar spectrum directly. However, there was an intensity loss from the incoming sunlight due to absorption caused by the UC-layer. To overcome this problem, UC particles were used in the reflecting layer or between the reflecting layer and the counter electrode (CE). Sunlight went through the photoanode and then excited the UC-layer [15,16]. The visible light emitted by the UC-layer was reflected back into the DSSC (Fig. 1b). In this case, the light which is transparent to DSSC (major in NIR region) can excite the UC particles and partial lost energy can be recovered. In addition, a combination of UC particles and normal photoanode material as a single-layer or double-layer photoanode has been reported (Fig. 1c) [17–20]. In this design, external loss can be avoided. However, as an addition, appropriate UC particles that can efficiently work with the normal photoanode material but does not interfere with favorable conduction of the photoanode can hardly be found. Besides, UC-particles as a reflector and energy relay material can effectively enhanced the light harvesting and efficiency of the cells. Recently, GY Chen extend the use of the energy relay process for harvesting light in the NIR region with NIR absorption and radiate visible upconverted emission, and the energy of which can then be radiative or nonradiative transferred to the dye sensitizer [11]. However, in their paper, Z907 which can absorb the longest wavelength of 750 nm can absorb both the green and red emission, but all the UC-emitting peak decrease. And cubic Er, Yb-$NaYF_4$ with average diameters of about 7 nm was utilized for doping into the 10 nm-pores of the TiO_2 film. Here, we report a simple modification with Er, Yb-YF_3 for DSSC by attaching it onto the surface of the TiO_2 film. And we found that, with N719 (maximum absorption at *ca.* 540 nm), UC-emission of Er, Yb-YF_3 occurring interesting changes, which lead to that the green peak decreased significantly with the red emission little changed. This can prove the fluorescence resonance energy transfer in UC-DSSCs with Er, Yb-YF_3, directly. After modification, power conversion efficiency (PCE) of 6.76% was achieved with the blank DSSC of 5.18%, which is an increase of 30.50%. It can be directly observed an NIR light-to-electricity property by SPS and IPCE characterizations.

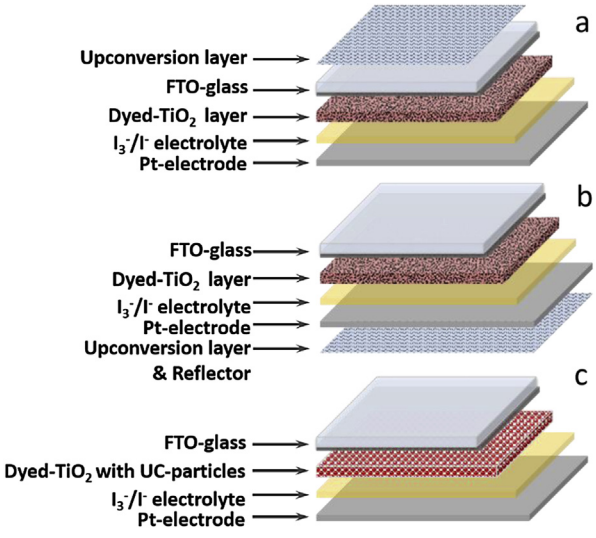

Fig. 1. Typical schematic structural diagram of a DSSC with upconversion layers designed and reported before.

2. Experimental section

2.1. Preparation of Er, Yb-YF_3

Er, Yb-YF_3 phosphors samples were synthesized by a hydrothermal method similar to the literature [21]. All the chemicals were of analytical grade and used as received without further purification. Stoichiometric Y_2O_3, Yb_2O_3 and Er_2O_3 were firstly dissolved in HNO_3 and then transferred into an oven overnight. Then 10 mL distilled water, 0.01 mol NaF and 0.09 mol NH_4HF_2 were added into the container. The pH value was adjusted to 3 by adding aqua ammonia dropwise. The suspension was transferred into Teflon-lined stainless steel autoclaves, sealed and maintained at 220 °C for 24 h. After natural cooling, the precipitates were centrifuged several times, washed with distilled water and ethanol to remove the ionic remnants, and dried at 70 °C for 8 h. However, similar process to the literature leads to none $NaYF_4$ but YF_3. In our opinion, it is due to the treatment of nitric acid which dissolved the rare earth oxides. In our process, the nitric acid were completely removed by dry the solution in an oven to completely dry. However, in the literature, the nitric acid was retained to the next-step. Thus, the slight difference in the process leads to a different product. To be assembled onto DSSCs, UC-YF_3 was dispersed into EtOH, and the solution was dropped onto the photoanode film of TiO_2 to form an attachment layer. Finally, the modified photoanodes were sintered in a muffle at 450 °C.

2.2. Characterization

Powder X-ray diffraction (XRD) patterns were recorded in the 2θ range of 10–70° using Cu-Kα radiation by Shimadzu XRD-6000 X-ray Diffractometer. Luminescence spectra were measured by the Edinburgh FLSP920 combined steady state fluorescence, using a 980 nm laser as the excitation source. The SPS instrument was assembled by Jilin University, monochromatic light was obtained by passing light from a 500 W xenon lamp (CHF-XQ500W, China) through a double-prism monochromator (SBP300, China), and the signals were collected by an SR830 DSP lock-in amplifier (Stanford).

2.3. Photoelectrochemical measurements

Optically transparent electrodes were made from an F-doped SnO_2-coated glass plate purchased from Acros Organics, Belgium. TiO_2 film was fabricated using a screen printing method. The photoanode films of commercial P25 were immersed in a 0.3 mM

N719 (Solaronix SA, Switzerland) in absolute ethyl alcohol for 24 h at room temperature. The electrolyte composed of 0.05 M I_2, 0.5 M LiI, and 0.1 M TBP in 1:1 (volume ratio) acetonitrile–propylene carbonate was admitted by capillary action. Photocurrent–photovoltage curves were recorded by CHI660D electrochemical analyzer (Chenhua, China). The light intensity of AM 1.5G global sunlight from a filtered 500 W xenon lamp (CHF-XM500, Changtuo, China with an AM 1.5G global filter from Newport) was calibrated by a standard Si solar cell (calibrated by National Institute of Metrology, P. R. China). All characterizations were carried out under ambient pressure and temperature. Based on the *J–V* curve, the fill factor (*FF*) is defined as:

$$FF = (J_{max} \times V_{max})/(J_{SC} \times V_{OC}) \quad (1)$$

where J_{max} and V_{max} are the photocurrent density and photovoltage for maximum power output, and J_{SC} and V_{OC} are the short-circuit photocurrent density and open-circuit photovoltage, respectively.

PCE is the overall power conversion efficiency (P_{in} is the power of incident light which is 100 mW cm^{-2} in this work) defined as

$$PCE = (FF \times J_{SC} \times V_{OC})/P_{in} \quad (2)$$

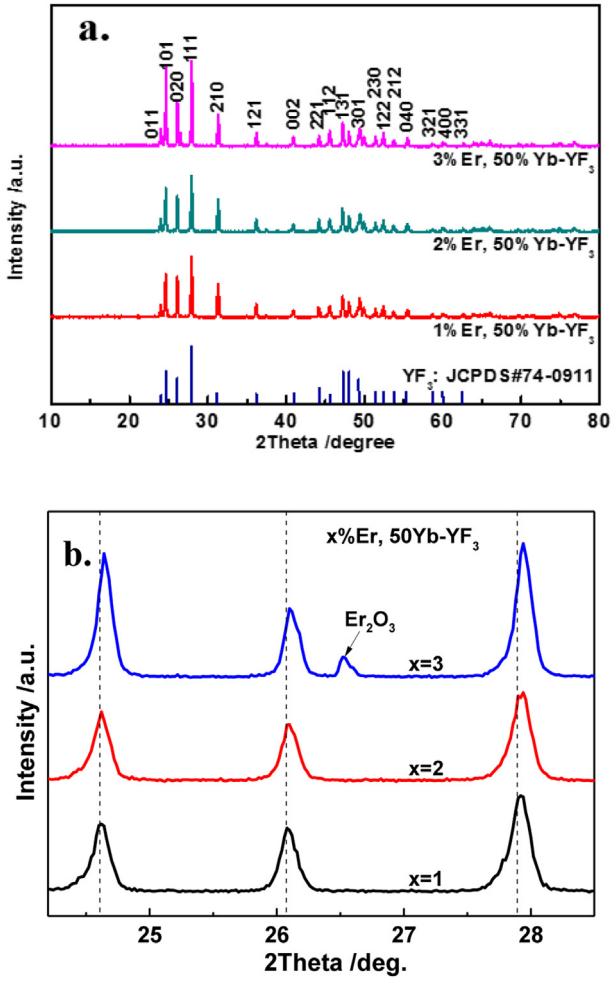

Fig. 2. The XRD patterns of Er, Yb-YF_3 (a: the whole pattern; b: magnifying detail).

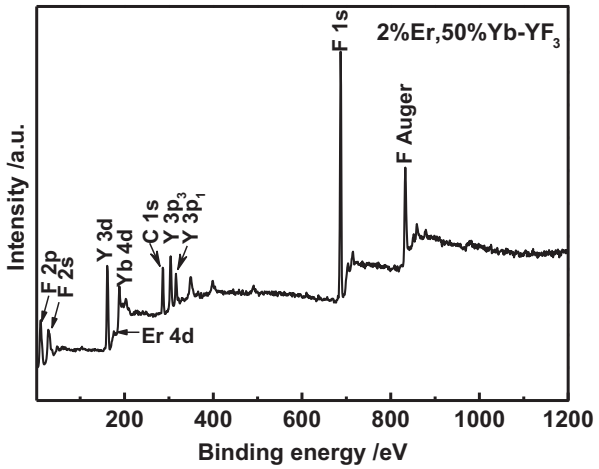

Fig. 3. The XPS spectrum of 2%Er, 50%Yb-YF_3.

3. Results and discussion

XRD pattern (Fig. 2a) of 2% Er, 50%Yb-YF_3 revealed main peaks corresponding to the pure orthorhombic phase for YF_3 [space group Pnma (62)], complying with JCPDS#74-0911. XRD peaks of ErF_3 and YbF_3 were not detected in the pattern.

Although the diffraction peaks of these samples are in the similar position, slight shift of the peaks can be observed when the patterns are magnified (Fig. 2b). Doping with Er^{3+} and Yb^{3+} ions does not lead to the crystal transformation. However, for Er^{3+} and Yb^{3+} ions, due to their smaller size than Y^{3+} ion (Er^{3+}: 0.089 nm, Yb^{3+}: 0.0868 nm and Y^{3+}: 0.09 nm), distortions can be found in the doped YF_3 lattice network. According to the Bragg equation ($2d\sin\theta = n\lambda$), when smaller Er^{3+} and Yb^{3+} ions substitute for Y^{3+} ion, lattice distortions lead to the decrease of interplanar distance. Thus, the corresponded diffraction peaks shift to the larger-angle direction. Besides, as the amount of doping ions increase, the shifting degree increases. The crystal distortions also provide evidence that Er^{3+} and Yb^{3+} ions are introduced into the lattice. However, when the concentration of Er^{3+} ions increased to 3%, impurity of Er_2O_3 can be found due to the newly-presented peak which corresponds to Er_2O_3.

XPS measurements were conducted to identify the composition and chemical states of Er, Yb-YF_3 (Fig. 3). The Er, Yb-YF_3 is mainly composited of Y, F, Er, Yb and C element. For Y 3d, two peaks are detected at 160.5 and 162.54 eV (Fig. S1a), which correspond to Y 3d5/2 and Y 3d3/2, respectively. The binding energies shift towards the higher energy compared to those of pure YF_3 (159.8 and 161.3 eV for Y 3d5/2 and Y 3d3/2, respectively). Thus, we assumed that Er^{3+} and Yb^{3+} doping had affected the chemical states of YF_3 by means of the substitution for Y. As presented in Fig. S1b, the F 1s peak is located at 687.0 eV. The broad peak at 169.3 eV (Fig. S1c) is identified as Er 4d, indicating the presence of Er in the sample. Yb^{3+} ions show a broad peak around 188.0 eV and it is identified as Yb 4d (Fig. S1d). Since ErF_3 and YbF_3 is not observed (as shown in Fig. 2a), it is certain that Er and Yb ions had been successfully implanted into the YF_3 lattice during the doping process. Therefore, it can confirm that Er^{3+} ions are incorporated into the YF_3 lattice and exist in a trivalent state.

To investigate the UC properties of Er^{3+}–Yb^{3+} couple in YF_3 crystal network, a series of samples were prepared with a fixed Yb^{3+} concentration at 50% and various Er^{3+} concentration (1, 2, 3 mol%). Fig. 4 shows the emission spectra of YF_3: Er^{3+}, Yb^{3+} phosphors under identical measurements conditions. Upon excitation with a 980 nm laser device, all the emission peaks observed

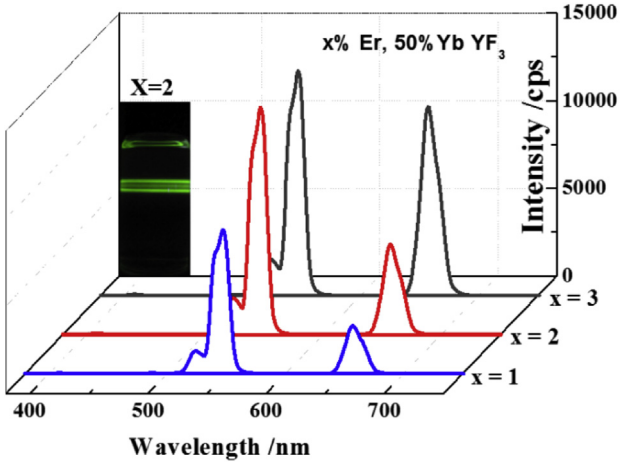

Fig. 4. UC luminesce spectra of x%Er, 50%Yb-YF_3 ($x = 1, 2, 3$) under 980 nm excitation (The emitting image is shown as the inset. Peaks centered at 522 nm, 541 nm and 655 nm correspond to Er^{3+}: $^2H_{11/2} \rightarrow {}^4I_{15/2}$, $^4S_{3/2} \rightarrow {}^4I_{15/2}$ and $^4F_{9/2} \rightarrow {}^4I_{15/2}$ transitions, respectively).

are consistent with the known transitions reported [15]. For example, the strongest pair of green emissions at 522 and 541 corresponds to the $^2H_{11/2} \rightarrow {}^4I_{15/2}$ and $^4S_{3/2} \rightarrow {}^4I_{15/2}$, respectively. Similarly, the red emission band around 655 nm is ascribed to the $^4F_{9/2} \rightarrow {}^4I_{15/2}$ transition. As the Er^{3+} concentration increases, both the green and the red peaks increases. However, when the Er^{3+} concentration reaches 3%, the green peak shows little increase and the red peak continues to grow. This is due to the saturation of Er^{3+}. When Er^{3+} concentration increases beyond 2%, an impurity of Er_2O_3 appears and the actual concentration is lower than 3% (similar to 2%). In Fig. 4, the inset shows the image of the green emission of 2%Er, 50%Yb-YF_3 suspended in EtOH. For DSSCs, this is a suitable UC process since it absorbs NIR radiation around 980 nm and emits 522, 541 and 655 nm light, for which DSSCs have high internal collection efficiency.

Based on the aforementioned discussions, the possible UC mechanism for Er, Yb-YF_3 phosphors upon excitation of a 980 laser device is schematically depicted in Fig. 5. The Yb^{3+} ions have only one excited state and are ideal sensitizer for Er^{3+} because of the relatively high oscillator strength of the $^2F_{7/2} \rightarrow {}^2F_{5/2}$ transition and the fact that Er^{3+} has a state with similar energy ($^4I_{11/2}$), which is

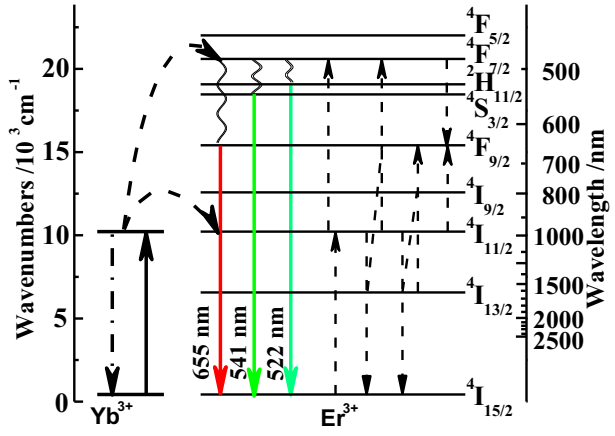

Fig. 5. Energy level diagram of Er^{3+} ($4f^{11}$) and Yb^{3+} ($4f^{13}$) couple showing several possible mechanisms for UC emitting, corresponding to the UC luminesce spectra under 980 nm excitation.

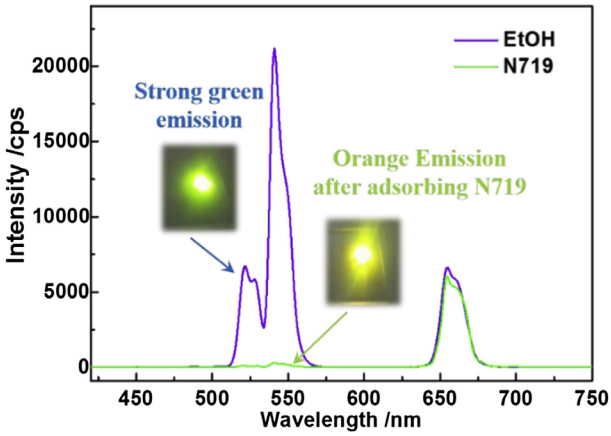

Fig. 6. UC luminesce spectra of 2%Er, 50%Yb-YF_3 in N719 and EtOH solution under 980 nm excitation (inset: the emitting image).

populated by energy transferred from Yb^{3+}. Under 980 nm excitation, incident lower-energy NIR photons promote Yb^{3+} ions from the ground state $^2F_{7/2}$ to the excited state $^2F_{5/2}$. Subsequent energy was transferred to an Er^{3+} ion to populate $^4I_{11/2}$ level, and then a second process occurred again to the same Er^{3+} ion to populate $^4F_{7/2}$ level which was called a two-photon process. As a result of fact that at least two photons are required to obtain upconverted light the emitted power is quadratically related to excitation power. Then, through nonradiative transition, $^2H_{11/2}$, $^4S_{3/2}$ and $^4F_{9/2}$ levels are populated. A subsequent radiative transition finally to the ground state ($^4I_{15/2}$) takes place with the emission of 522, 541 and 655 nm, respectively. Furthermore, energy transfer of Er^{3+} ions may happen via transitions (Er^{3+}: $^4I_{11/2} \rightarrow {}^4I_{15/2}$) and ($Er^{3+}$: $^4I_{11/2} \rightarrow {}^4F_{7/2}$). Both of the two green upconversion (522 and 541 nm) mechanisms can be also relaxation from the $^4F_{7/2}$ level. For the red emission, a CR (Cross Relaxation) process via transition ($^4I_{11/2} \rightarrow {}^4I_{15/2}$) and ($^4I_{13/2} \rightarrow {}^4F_{9/2}$) can take place, too. Besides, there exists another possible process to populate the $^4F_{9/2}$ level in which two Er^{3+} ions, one of them in the $^4I_{11/2}$ level and the other one in the $^4F_{7/2}$ level, interact and go both to level $^4F_{9/2}$.

After investigating the solid UC emission of 2%Er, 50%Yb-YF_3, considering the actual working environment in DSSC, a UC emission of 2%Er, 50%Yb-YF_3 in the sensitizer solution (N719 in absolute EtOH, *ca.* 10^{-5} M) was tested. As a reference, 2%Er, 50%Yb-YF_3 in absolute EtOH was also tested. Interesting phenomena were found after irradiating the solution with 980 nm laser device. In the insets of Fig. 6, it shows two images corresponding to UC-YF_3 in the two solutions respectively. In EtOH solution, 2%Er, 50%Yb-YF_3 shows a strong green emission as solid state. However, when in the N719 solution, the green emission changes into an orange emission which indicates the red emission becomes visibly stronger or the green emission becomes much weaker. The UC emitting spectra prove the phenomenon. In Fig. 6, significant decrease of the green emitting peak can be found. In contrast, the red emitting peak decreases little.

Fluorescence resonance energy transfer (FRET) is an excited state interaction in which emission of one fluorophore is coupled to the excitation of another. It occurs primarily because the acceptor dipole interacts or resonates with the donor dipole in the range of 1–10 nm. The excitation energy can be transferred by a radiationless process to a neighboring fluorophore if their energy level difference corresponds to the quantum of excitation energy. In this process, the quantum, or exciton, is transferred, which raises the electron in the acceptor to a higher energy state as the photo-excited electron in the donor returns to ground state. This

mechanism requires resonance interaction between donor and acceptor over distances greater than interatomic. In this paper, 2% Er, 50%Yb-YF_3 adsorbed N719 molecular like TiO_2, which indicated that the distance between the donor and acceptor molecules is less than 10 nm. To our knowledge, N719 is a common sensitizer with the strongest visible absorption of *ca.* 540 nm (Fig. S2). It can be seen that the absorption band with the peak at *ca.* 540 nm corresponds well with the green upconversion photoluminescence band. For the green emitting peak, the emission intensity decreased significantly after the addition of the 10^{-5} M N719 dye, while for the red emitting peak, little decrease is observed, indicating that the energy transfer from green emitting peak is much more efficient than from the red emitting peak. It should be noted that the green emitting peak is the main PL peak of the UC particles used herein, which is crucial for enhancing the energy transfer efficiency. According to the quantitative theory for energy transfer developed by Theodor Förster [22], FRET efficiency, E can be obtained by measuring the fluorescence intensities of the donor with acceptor, F_{da} and without acceptor, F_d [23,24]:

$$E = 1 - F_{da}/F_d \quad (3)$$

FRET efficiency can also be measured using the lifetime or quantum yield of the donor in presence, T_{da} or τ_{da} and absence of the acceptor probe, T_d or τ_d:

$$E = 1 - T_{da}/T_d \quad (4)$$

or

$$E = 1 - \tau_{da}/\tau_d \quad (5)$$

According to the fluorescence intensities, FRET efficiency was calculated and listed in Table 1.

As shown in Table 1, for the green emission centered at 522 and 541 nm, it presents an efficiency as high as 0.982 and 0.986 respectively, which indicates the high-efficient energy transfer from the donor, UC-YF_3 phosphor to the acceptor, N719 molecules. For the green peaks, the emission intensity decreased 53 times after the addition of the 10^{-5} M N719 dye, while for the red peak, little decrease is observed, indicating that the energy transfer from green peaks is much more efficient than from red peak. Considering the color change, the peak intensity ratios of green peaks and red peak were calculated (Table 1). The absorption spectrum of the N719 dye is shown in Fig.e S2. It can be seen that the absorption band with the peak at *ca.* 540 nm corresponds well with the 541 nm UC-photoluminescence (UCPL) band. When UC-YF_3 was dispersed in absolute EtOH without N719, F_{522}/F_{541} is 3.16, however, when it was dispersed in N719 solution, F_{522}/F_{541} decreased to 2.57. It indicates that the peak of 541 nm changed more, due to the closer relationship between the 541 nm emission of UC-YF_3 and 540 nm absorption of N719. The result agrees with the FRET efficiency, which shows a value of 0.986 for 541 nm larger than that of 0.982 for 522 nm. As discussed above, green emission is the most major emission for UC-YF_3, and the phosphor shows a green light when excited under 980 nm laser. However, for the red emission centered at 655 nm, the energy transfer efficiency is 0.091, which is about 1/10 that of the green emission energy transfer efficiency, which indicates that it is not convenience for FRET. And both the values of F_{522}/F_{655} and F_{541}/F_{655} shows a significant decrease with N719 (F_{522}/F_{655}: 1.01 → 0.02; F_{541}/F_{655}: 3.20 → 0.05). Thus a result of FRET, UC-YF_3 in N719 solution shows an orange light (rather than green light) under 980 nm laser.

Table 1
Parameters of FRET process.

	F_{ad}[a]	F_d[b]	F_{ad}/F_d	E
522 nm	122.13	6699.75	0.018	0.982
541 nm	313.82	21196.59	0.014	0.986
655 nm	6026.89	6629.57	0.909	0.091
	F_{541}/F_{522}	F_{541}/F_{655}	F_{522}/F_{655}	
With N719	2.57	0.02	0.05	
Without N719	3.16	1.01	3.20	

[a] ad: UC particles with N719.
[b] d: UC particles alone without N719.

To investigate the interaction of UC particles and P25, the UCPL properties of the sintered and non-sintered films were test, and the spectra were presented in Fig. 7. As shown in Fig. 7, before sintered, the film presented a typical UCPL spectrum of solid UC-YF_3, which means that P25 does not affect the UCPL properties. However, after sintered, the film showed a similar spectrum which was much lower than the non-sintered one. The result was quite similar to the FRET process in N719 solution. However, there was no overlap of emission spectra of UC-YF_3 (>522 nm) and absorption spectra of P25 (<380 nm). Hence, there could be no FRET occurs between P25 and UC-YF_3. We noticed a report that Chang et al. found a phenomena that when sintered with TiO_2 at 450 °C, UC-$NaYF_4$ can share the interface with TiO_2, and the direct injection from UC particles to TiO_2 becomes feasible[25]. The results show remarkably consistent with ours. Thus the intensity loss of the film after sintered can be attributed to the electron injection from UC-YF_3 to TiO_2. Different from the FRET process, there is no overlap limit, and all the emitting peaks would become weaker. For the green peak at 522 nm, it shows an intensity of 516.84 before sintered and 57.44 after sintered, which shows a loss of 88.89%. For the strongest peak at 541 nm, it shows an intensity loss of 92.97% from 2215.51 to 155.76 after sintered. Among them, peak at 655 nm shows the least loss (83.11%) and the peak is set as a datum peak. The value of I_{522}/I_{655} and I_{541}/I_{655} can show the emitting color of the film. When the value is getting bigger, the color turns to green, and in the contrast, the color would turns into orange and even red. Before sintered, I_{522}/I_{655} and I_{541}/I_{655} is 1.85 and 7.91, respectively, and after sintered, the value turns into 1.21 and 3.29, respectively, which means that the emitting color of the film under 980 nm laser becomes more orange/red from green. The decrease of I_{522}/I_{655} and I_{541}/I_{655} is 34.59% and 58.41%, respectively. Thus, the energy level of 541 nm is more convenient to inject the excited electrons into the conductive band of TiO_2.

To present a clear and visible process for UC-YF_3 in DSSC, a scheme was shown in Fig. 8 with a CIE image. For UC-YF_3 alone in

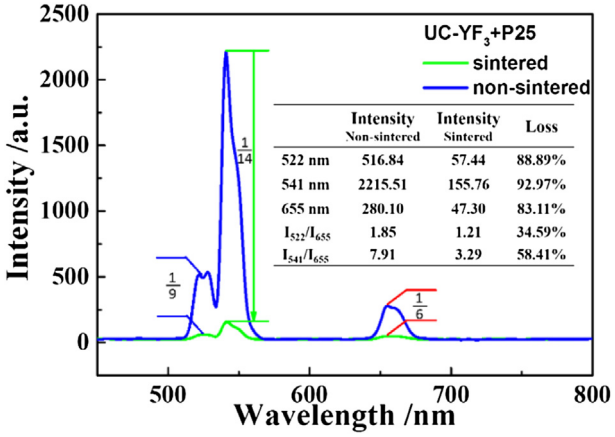

Fig. 7. UC luminesce spectra of sintered and non-sintered 2%Er, 50%Yb-YF_3/P25 film under 980 nm excitation.

solid state or EtOH solution, UC-YF_3 can absorb NIR light *ca.* 980 nm and emit visible light of green and red (Fig. 8a). However, when dispersed into N719 solution, the green emission is cut off and a green FRET process happens instead (Fig. 8b). As a result, the N719 dye can be excited by a red LET process and a green FRET. Besides, when UC-YF_3 is sintered with P25 powder at 450 °C as in DSSC photoanode film, the green emission is also cut down. However, there is no proper donor for a FRET process like Fig. 8b. Thus, there might be another path for the energy transfer. According to Chang's report and the UCPL properties of the film, when sintered with TiO_2 at 450 °C, UC-YF_3 can share the interface with TiO_2, and the direct injection from UC particles to TiO_2 becomes feasible (Fig. 8c). Hence, in conclusion, Fig. 8d shows the overall process occurring in the DSSCs with UC-YF_3 as attachment layer under NIR light. Red-LET, green-FRET and electron injection cooperated with each other to enhance the performance of DSSC. Fig. 8e shows the CIE image of UC-YF_3 in different state. As shown in Fig. 8e, pure UC-YF_3 as solid powder, UC-YF_3 dispersed into EtOH and UC-YF_3 mixing with P25 show similar CIE points, which locate in the green region. When dispersed into N719 solution, the location changes greatly towards the red direction. However, when sintered with P25, the location changed towards the light green direction. The two different changes attribute to the two different processes and also the efficiencies. According to the spectra and the CIE image, the energy transfer efficiency of FRET is much higher than that from UC-YF_3 to P25.

The noncontact technique for surface-state distribution named the surface photovoltage spectrum method is applied to characterize the anode material of dye-sensitized solar cells. In order to study the effect of UC phosphor on the overall performance of the cells, surface photovoltage response of cells with and without Er, Yb-YF_3 was tested. As shown in Fig. 9, the SPS analysis for DSSC with Er, Yb-YF_3 samples demonstrates a typical characteristic response peak at *ca.* 340 nm which can be assigned to the band–band electron transition of TiO_2. The broad response from 400 to 700 nm can be assigned to the dye-sensitization of N719. However, a new response from 950 to beyond 1000 nm appears with attachment of Er, Yb-YF_3, which provides proof that the upconversion work in the DSSC in the NIR region. Most possibly, FRET can significant enhance the energy transfer efficiency compared with the LET process (Luminescence-mediated energy transfer), due to the non-directional scatter propagation of LET. When NIR was absorbed

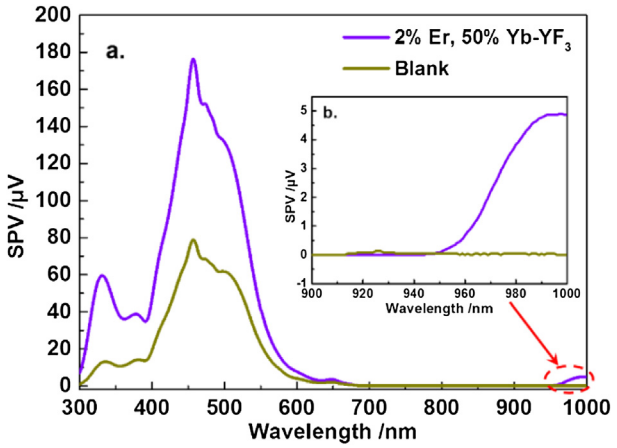

Fig. 9. Surface photovoltage spectra of a dye sensitized solar cell with and without Er, Yb-YF_3 attachment layer from 300 to 1000 nm. Insert: near-IR region.

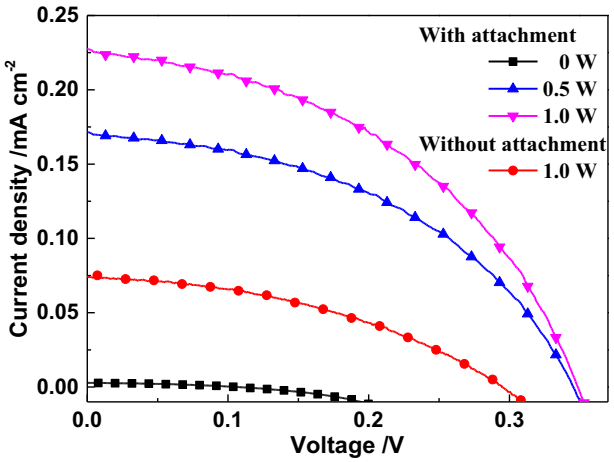

Fig. 10. *J–V* characteristics of DSSCs with and without the attachment of UC-YF_3 under illumination of a 980 nm laser.

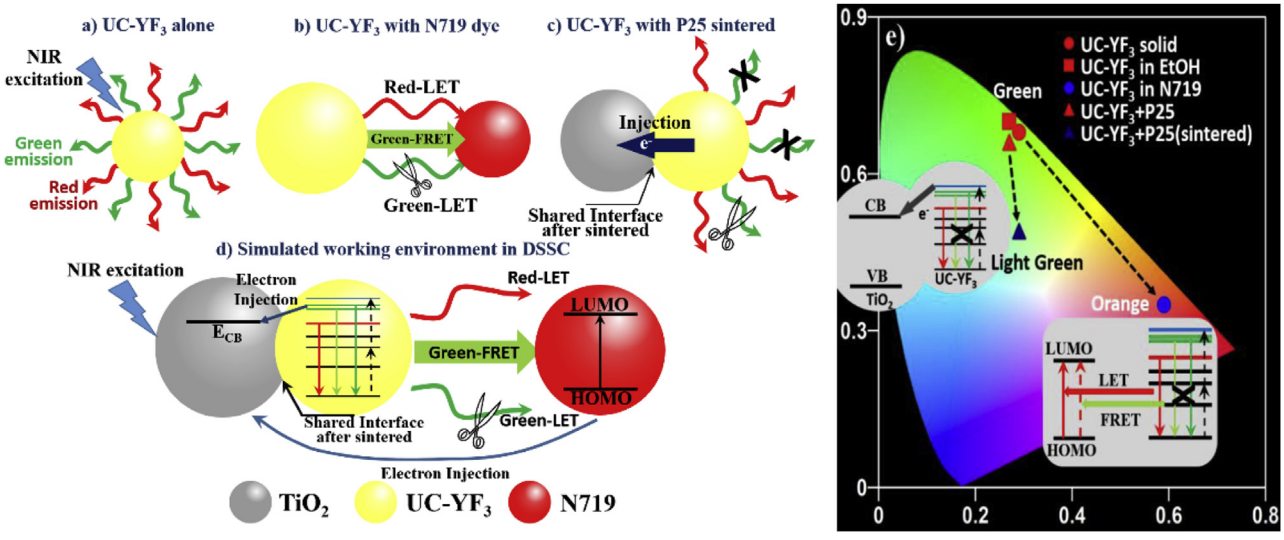

Fig. 8. Possible energy transfer of UC-YF_3 in DSSC and the CIE image of UC-YF_3 with and without FRET process.

by Er, Yb-YF_3 attachment, upconversion process happened. However, due to adsorption of N719, FRET happened with the result of radiationless energy transfer take the place of LET, and N719 was directly excited. Thus a significant response can be found in Fig. 8. And for DSSC with Er, Yb-YF_3 attachment, it shows a much stronger signal throughout the whole region, due to the scattering effect of the attachment.

3.1. Solar cell performance

In order to demonstrate unequivocally that indeed the attachment of the UC-YF_3 leads to photocurrent generation via the upconversion of NIR light, the *J–V* response of both DSSCs with and without the attachment layer of UC-YF_3 were measured under the illumination of a 980 nm laser. The *J–V* curve of the cell attached with Er, Yb-YF_3 is shown in Fig. 10. The short circuit photocurrent under 1.0 W irradiation intensity is 0.23 mA cm^{-2} with V_{OC} value of 0.348 V. And with 0.5 W power supply, 0.345 V of V_{OC} and 0.17 mA cm^{-2} of J_{sc} were obtained. Without the laser, a slight current was also found, which corresponded to the dark current. The *J–V* curve of the control device without the UC-YF_3 attachment layer also was measured under illumination with the 980 nm laser. However, for the blank DSSC under 1.0 W power irradiation, only 0.07 mA cm^{-2} of J_{sc} and 0.294 V of V_{OC} were obtained in this case. Thus, the generated photocurrent can be solely contributed to the NIR light harvesting via the UC-YF_3 layer modified DSSC. The advantage of attaching the UC-YF_3 is the simultaneous in situ NIR light upconversion and direct absorption of the emitted light by the dye via FRET.

Fig. 11 compares the photocurrent density–voltage (*J–V*) properties of DSSC with UC-YF_3 before and after sintered under simulated AM 1.5G light. And the detailed Parameters of DSSCs with and without UC-YF_3 are listed in Table 2. As the amount of UC-YF_3 increases, the PCE of the cells shows an increasing trend. The highest PCE reaches 6.22% with the amount of 4 drops. The open circuit voltage swings around 0.697 V. The performance of DSSC is improved with the attachment of UC-YF_3. As aforementioned discussion, UC-YF_3 works with an upconversion FRET, scattering effect and LET process. It makes DSSC can utilize the NIR light, and the scattering effect can improve the efficiency of light absorbing.

However, when the photoanode with the attachment of UC-YF_3 was sintered, all the parameters increase. And the highest PCE reaches 6.76% with an increase of 43.5% compared with the blank DSSC. At comparable amount of UC-YF_3, the performance of the sintered DSSC improves, compare with DSSC with the attachment without sintering. For example, at the amount of 5 drops (Fig. 12), the current density shows an enhancement of 30.18%. And the open circuit shows an increase from 0.687 to 0.721 V. IPCE spectra were measured to confirm the improvement of DSSC with UC attachment. As shown in Fig. 13, both the two types of DSSCs show a typical IPCE curve with a maximum around *ca.* 520 nm. For DSSCs with UC-YF3, due to the scattering effect, the whole IPCE in the visible region grows higher than that of the blank DSSCs. In addition, there appears a new IPCE response signal around *ca.* 980 nm, which can correspond to the SPV spectra in Fig. 9. And the IPCE curves can confirm the contribution of UC-YF3 in DSSC for the NIR conversion.

There are two possible reasons to explain the improvement: ① sintering can make TiO_2 film much tighter with the attachment and

Table 2
Parameters of DSSC with and without UC-YF_3.

Samples	J_{SC} (mA cm^{-2})[a]	V_{OC} (V)	FF	PCE (%)
Blank	12.88	0.677	0.59	5.18
2-drop	13.05	0.707	0.61	5.67
3-drop	12.52	0.689	0.61	5.26
4-drop	15.20	0.697	0.59	6.22
5-drop	12.36	0.687	0.63	5.34
2-drop (sintered)	12.90	0.698	0.60	5.42
3-drop (sintered)	13.95	0.702	0.64	6.25
4-drop (sintered)	15.00	0.698	0.64	6.69
5-drop (sintered)	16.09	0.721	0.58	6.76

[a] The active area of the photoanodes is 0.25 cm^2.

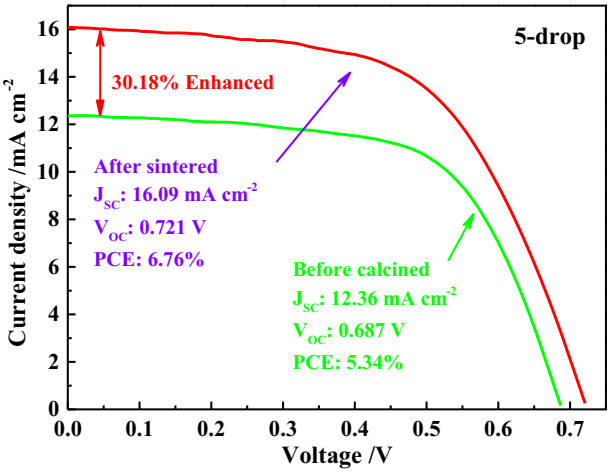

Fig. 12. The *J–V* curves of the cells with 5 drops of 2%Er, 50%Yb-YF_3 under simulated AM 1.5G irradiation before sintered and after sintered.

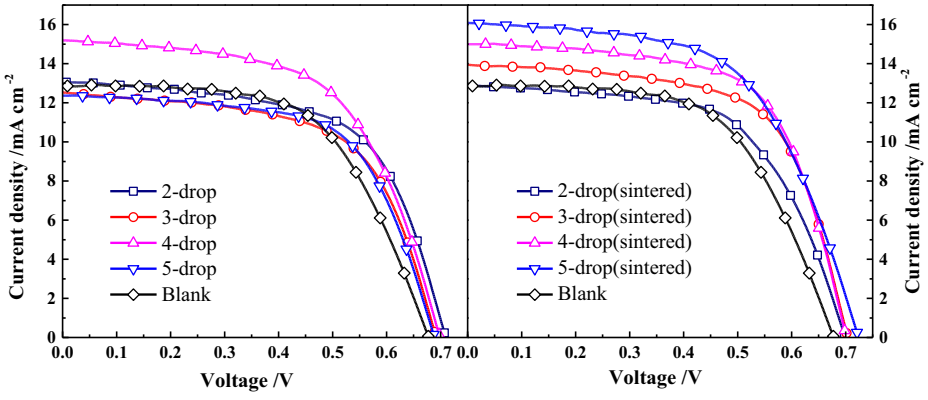

Fig. 11. The *J–V* curves of the cells with increasing amount of UC-YF_3 under simulated AM 1.5G irradiation (left: before sintered; right: after sintered).

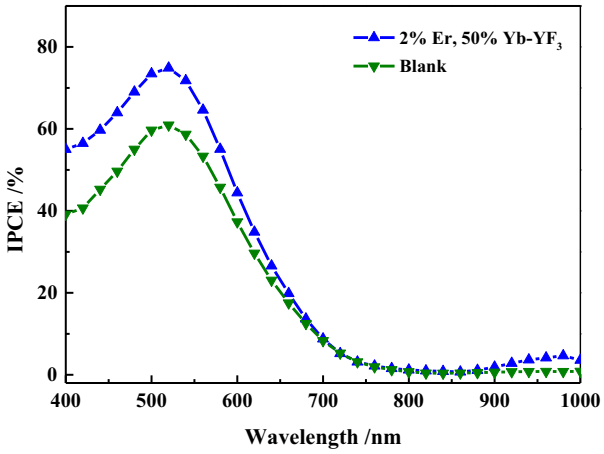

Fig. 13. IPCE curves of the cells with 5 drops of 2%Er, 50%Yb-YF_3 under simulated AM 1.5G irradiation before sintered and after sintered.

it benefit the FRET; ② sintering can lead to a shared interface between TiO_2 and UC-YF_3, and it makes UC-YF_3 can directly inject the electrons (excited by the NIR light in the upconversion process) into TiO_2 network [25]. The detail process in the DSSC is presented in Fig. 14.

4. Conclusions

In summary, in this report, we investigated the effect of UC-YF_3 introduced through a simple method in photovoltaic devices. They were found to enhance the light harvesting efficiency of dye sensitized solar cells (DSSCs) under both near-IR light and sunlight effectively. With the attachment of UC-YF_3, DSSC showed a photocurrent density of 0.23 mA cm^{-2} under 980 nm laser of 1 W, which is 3 times that of blank devices without UC-YF_3. We observed that the utilization of UC-YF_3 leads to an increase in the overall photocurrent of the cells under simulated sunlight irradiation (5.18% → 6.22%). It is suggested that, apart from acting as an upconversion material to harvest the near-IR light, the UC-YF_3 can serve as a scattering material to enhance the absorbance of the cells. On the basis of the aforementioned results, DSSCs with UC attachment were sintered at 450 °C, and a further improved PCE was achieved. The PCE value was increased from 5.34% to 6.76%. Finally, working mechanism of UC-YF_3 in photoanode was observed in this report: ①Fluorescence resonance energy transfer (FRET); ②Luminescence-mediated energy transfer (LET); ③Electron injection into TiO_2; ④Scattering effect.

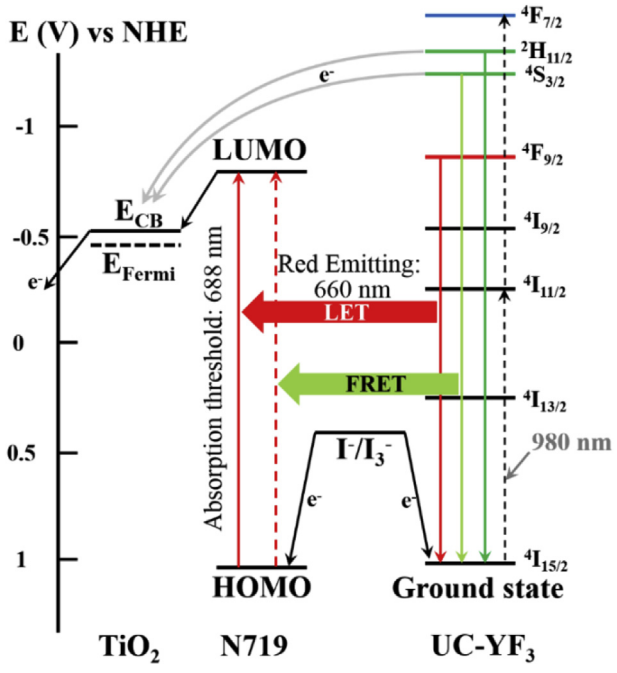

Fig. 14. Energy level diagram of the UC-YF_3, N719 dye and TiO_2, and the energy level of the redox couple (I_3^-/I^-), showing the electron transfer from the UC-YF_3 to the CB of TiO_2, I_3^-/I^- to the ground state of the UC phosphor, and energy transfer from the UC phosphor to the N719 dye under irradiation with NIR light. LUMO = lowest unoccupied molecular orbital. HOMO = highest occupied molecular orbital. E_{CB} = energy of the conduction band of TiO_2. E_{Fermi} = Fermi level.

Acknowledgments

This work was supported by National Natural Science Foundation of China (Grant 21171044 and 21371040), the National key Basic Research Program of China (973 Program, No. 2013CB632900), and supported by Program for Innovation Research of Science in Harbin Institute of Technology.

Appendix A. Supplementary data

Supplementary data related to this article can be found at http://dx.doi.org/10.1016/j.jpowsour.2014.04.100.

References

[1] B. O'Regan, M. Gratzel, Nature 353 (1991) 737–740.
[2] M. Gratzel, Nature 414 (2001) 338–344.
[3] F. Gong, H. Wang, X. Xu, G. Zhou, Z.S. Wang, J. Am. Chem. Soc. 134 (2012) 10953–10958.
[4] M. Gratzel, J. Photochem. Photobiol. C 4 (2003) 145–153.
[5] G.B. Shan, G.P. Demopoulos, Adv. Mater. 22 (2010) 4373–4377.
[6] M.D. Ye, H.Y. Liu, C.J. Lin, Z.Q. Lin, Small 9 (2013) 312–321.
[7] R. Levinson, P. Berdahl, H. Akbari, Sol. Energ. Mater. Sol. C 89 (2005) 351–389.
[8] R. Levinson, P. Berdahl, H. Akbari, Sol. Energ. Mater. Sol. C 89 (2005) 319–349.
[9] K. Hara, T. Sato, R. Katoh, A. Furube, Y. Ohga, A. Shinpo, S. Suga, K. Sayama, H. Sugihara, H. Arakawa, J. Phys. Chem. B 107 (2003) 597–606.
[10] W.M. Campbell, A.K. Burrell, D.L. Officer, K.W. Jolley, Coord. Chem. Rev. 248 (2004) 1363–1379.
[11] C.Z. Yuan, G.Y. Chen, P.N. Prasad, T.Y. Ohulchanskyy, Z.J. Ning, H.N. Tian, L.C. Sun, H. Agren, J. Mater. Chem. 22 (2012) 16709–16713.
[12] S. Chen, G.H. Zhou, F.F. Su, H.L. Zhang, L.X. Wang, M.J. Wu, M.B. Chen, L.K. Pan, S.W. Wang, Mater. Lett. 77 (2012) 17–20.
[13] J.V. Garcia, J.P. Yang, D.K. Shen, C. Yao, X.M. Li, R. Wang, G.D. Stucky, D.Y. Zhao, P.C. Ford, F. Zhang, Small 8 (2012) 3800–3805.
[14] A.F. Khan, R. Yadav, P.K. Mukhopadhya, S. Singh, C. Dwivedi, V. Dutta, S. Chawla, J. Nanopart. Res. 13 (2011) 6837–6846.
[15] X.F. Liang, X.Y. Huang, Q.Y. Zhang, J. Fluoresc. 19 (2009) 285–289.
[16] A. Moadhen, C. Bouzidi, H. Elhouichet, R. Chtourou, M. Oueslati, Opt. Mater. 31 (2009) 1224–1227.
[17] J. Zhang, H.O. Shen, W. Guo, S.H. Wang, C.T. Zhu, F. Xue, J.F. Hou, H.Q. Su, Z.B. Yuan, J. Power. Sources 226 (2013) 47–53.
[18] J.H. Wu, J.L. Wang, J.M. Lin, Z. Lan, Q.W. Tang, M.L. Huang, Y.F. Huang, L.Q. Fan, Q.B. Li, Z.Y. Tang, Adv. Energy Mater. 2 (2012) 78–81.
[19] L. Li, Y.L. Yang, M. Zhou, R.Q. Fan, L.L. Qiu, X. Wang, L.Y. Zhang, X.S. Zhou, J.L. He, J. Solid State Chem. 198 (2013) 459–465.
[20] J.L. Wang, J.M. Lin, J.H. Wu, M.L. Huang, Z. Lan, Y. Chen, S. Tang, L.Q. Fan, Y.F. Huang, Electrochim. Acta 70 (2012) 131–135.
[21] X.P. Chen, W.J. Zhang, Q.Y. Zhang, Phys. B 406 (2011) 1248–1252.
[22] F. Theodor, J. Biomed. Opt. 17 (2012) 011002-1–011002-10.
[23] V. Bernaid, B.S.N. Mário, Molecular Fluorescence: Principles and Applications, second ed., John Wiley & Sons, Weinheim, 2012.
[24] R.M. Clegg, Lab. Tech. Biochem. Mol. Biol. 33 (2009) 1–57.
[25] J. Chang, Y.H. Ning, S.L. Wu, W.B. Niu, S.F. Zhang, Adv. Funct. Mater. 33 (2013) 5910–5915.